Bearing capacity beneath tapered blades of open dug caissons in sand

Ronan Royston[1, 2], Bryn M. Phillips[1, 2], Brian B. Sheil[1], Byron W. Byrne[1]
[1] Department of Engineering Science, University of Oxford, UK
[2] Ward and Burke Construction, Kilcolgan, Co. Galway
Email: ronan.royston@eng.ox.ac.uk, bryn.phillips@hertford.ox.ac.uk, brian.sheil@eng.ox.ac.uk, byron.byrne@eng.ox.ac.uk

ABSTRACT: An open-dug caisson shaft is a form of top-down construction in which a concrete shaft is sunk into the ground using the weight of the shaft and additional kentledge, if required. Excavation at the base of the caisson shaft wall allows the structure to descend through the ground. A thorough understanding of the interaction between the caisson shaft and soil is essential to maintain controlled sinking of the caisson. In this paper, the failure mechanisms developed beneath caisson blades in sand are investigated. A series of laboratory tests were carried out at the University of Oxford to explore how varying blade angles affect the performance of the bearing capacity beneath the caisson. Cutting angles of 30°, 45°, 60°, 75° and 90° (flat) were penetrated into sand under plane strain conditions; forces were monitored using a Cambridge-type load cell while soil displacements were recorded using Particle Image Velocimetry (PIV) techniques. The aim of this study is to understand how the soil failure mechanism develops and to determine the optimum cutting angle. The results of the laboratory tests can be scaled to predict the likely behaviour in the field. Results show that the bearing capacity is significantly dependent on the cutting angle; in a dense sand a steep cutting angle may be used to aid sinking of the caisson.

KEY WORDS: Caisson; tapered blade; bearing capacity; laboratory testing.

1 INTRODUCTION

An open-dug caisson shaft is a form of top-down construction. They have many functions in industry such as launch and reception pits for tunnel boring machines and underground storage tanks for foul and storm water attenuation. Caissons can be sunk through various soil types including sand, clay and rock. It can be a very safe and efficient form of construction as the permanent structure is used to retain the soil and water during excavation as shown in Figure 1.

Figure 1 30 m diameter reinforced concrete caisson at Anchorsholme Park, Blackpool, constructed by Ward and Burke Construction

In order for a caisson to sink into the ground, both the skin friction that develops between the soil and the concrete shaft in addition to the bearing capacity of the soil beneath the shaft walls must be overcome. A common technique to aid the sinking process is the use of a tapered blade, or cutting edge, beneath the wall of the shaft. The purpose of the cutting edge is to cut into the ground, anchor the caisson horizontally and maintain verticality. It mobilises the failure mechanism of the soil towards the centre of the shaft, so that the soil in this area can be easily excavated to allow the caisson to sink. In order to achieve controlled sinking of the shaft, a thorough understanding of the bearing failure that develops in different soils is therefore essential. It ensures operatives in the field know where to excavate to induce bearing failure beneath the shaft walls. Moreover, a reduction in the bearing capacity beneath the caisson blades means less kentledge will be required to get the shaft to formation level.

The bearing capacity of sloped caisson footing depends on the angle of the tapered blade, roughness of the interface, angle of friction of the soil, width of the footing and the unit weight of the soil. In this paper it is assumed that the caisson diameter is large, 2D plane strains will develop with minimal conical action. While some work has been undertaken on sloped conical footings [1-2], limited information is available on 2D plane strain conditions for tapered footings.

Tomlinson [3] recommends various tapered angles depending on the soil type; flatter cutting angles are recommended for sand compared to clay. Nonveiller [4] describes various potential rupture surfaces. As the caisson penetrates into the soil, the resisting forces increase until a new state of equilibrium is achieved.

A method for quantifying the bearing capacity factor, N_γ, using limit-equilibrium theory was proposed to quantify the bearing capacity of tapered footings beneath caissons [5-6]. According to this approach, the value of N_γ is less sensitive to the angle of friction compared to the blade angle and embedment depth of the wall. However, some important parameters are neglected in this method, such as the interface friction between the soil and sloped blade of the caisson.

The aim of this study is to explore the performance of various tapered angles in sand through a series of laboratory tests. Particle image velocimetry (PIV) analysis is employed to track the failure planes developed in the soil during testing. In addition, a number of tests were carried out to examine the influence of overburden pressure during sinking.

2 EXPERIMENTAL EQUIPMENT

A three degree of freedom loading rig, developed at the University of Oxford [7], was used for the laboratory testing in this study (see Figure 2 and 3). A Cambridge-type load cell, attached to the end of the loading arm, records vertical, horizontal and moment reaction.

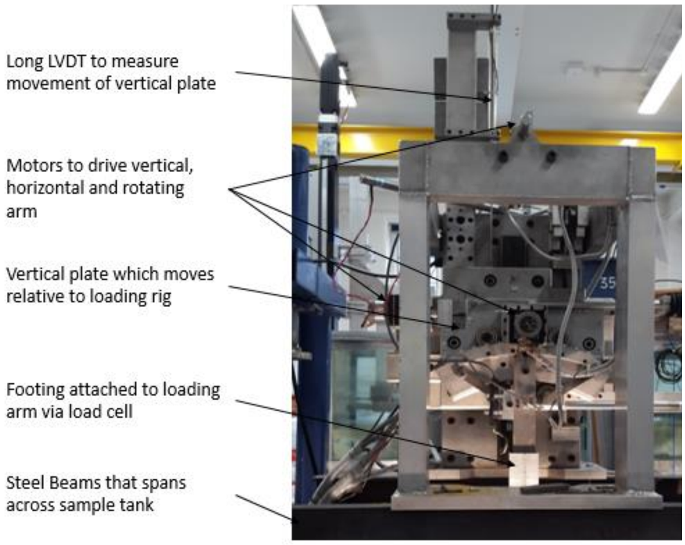

Figure 2 Three degree of freedom loading rig

The loading rig was located on top of a 600 mm x 300 mm x 95 mm testing tank which has a perspex front, which allows the sand movements to be recorded during testing, see Figure 4. A Nikon DS3200 camera located 700 mm from the front of the tank was used to capture images at a frequency of 1 Hz during testing. A downward penetration rate of 0.5 mm/sec was adopted for all tests; rate effects in sand are not expected to be significant. PIV analysis was carried out by processing the images using MATLAB module GeoPIV [8].

The experiments were conducted using a dry, yellow Leighton Buzzard DA30 silica sand, the properties of which are summarised in Table 1.

Table 1 Properties of Leighton Buzzard DA30 sand

Property	**Value**
D_{10}, D_{30}, D_{50}, D_{60}, D_{90}, (mm)	0.36, 0.45, 0.51, 0.54, 0.65
Specific Gravity, G_s	2.73
Minimum dry density, γ_{min} (kN/m^3)	14.5
Maximum dry density, γ_{max} (kN/m^3)	17.1
Critical state friction angle, ϕ'_{cs} (°)	32

Loose sand samples were prepared using a sand raining procedure in conjunction with a low drop height. Dense samples were prepared by vibrating the testing tank after sand raining. To ensure a repeatable bulk density was achieved for each sample, the tank was filled using the same drop height for all tests.

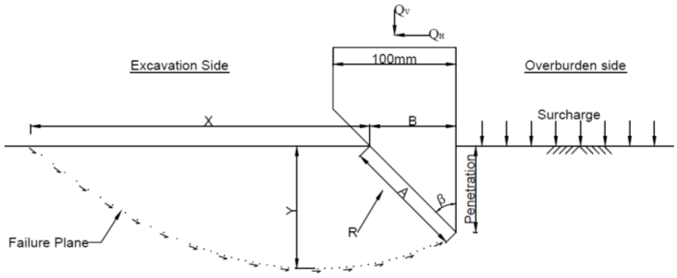

Figure 3 Test setup and soil failure wedge

A schematic of a typical cross section of a cutting edge and possible soil failure plane is provided in Figure 3, where B is the width at embedment, A is the length of the face, β is the tapered cutting angle, Q_V and Q_H are the vertical and horizontal reactions, R is the resultant reaction of the forces, and X and Y are the width and depth of the failure plane. It is worth noting that value of β generally used in industry is 45°, derived from on-site experience.

Aluminum pieces were created as the test pieces of varying cutting angles, β. In order to reduce the friction between the test pieces and the sides of the tank, 1 mm polytetrafluoroethylene (PTFE) sheets were placed either side of the piece with compressible foam placed in between the PTFE and the test piece. The test piece spanned the width of the test tank to ensure plane strain conditions.

Figure 4 Testing tank

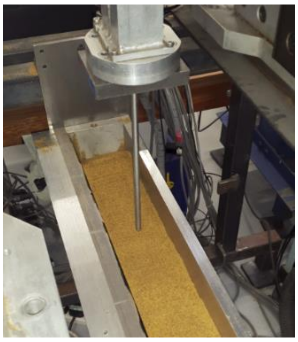

Figure 5 Cone Penetration

3 VALIDATION OF TESTING PROCEDURES

Cone tests were performed, with an 8 mm diameter cone and a 60° cone angle, to examine the uniformity of the sample. The cone was penetrated 150 mm into soil samples prepared with three different relative densities, I_D, as per Equation (1), where γ is the density of the prepared sample. The cone was attached to the rig as shown in Figure 5 and penetrated through the sand at a rate of 1 mm/s. From the results presented in Figure 6, the cone penetration resistance appears consistent with depth thus indicating a uniform sample. Moreover, it is obvious that at higher relative densities, there is a commensurate increase in the cone resistance.

$$I_D = \frac{\gamma_{max}}{\gamma}\left(\frac{\gamma - \gamma_{min}}{\gamma_{max} - \gamma_{min}}\right) \quad (1)$$

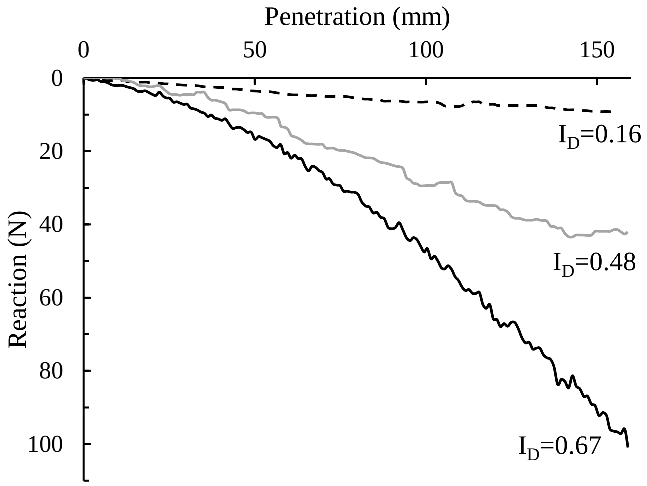

Figure 6 Cone penetration results

A series of preliminary tests were carried out to validate the present sand properties, sample preparation and experimental techniques. Careful consideration of the stress level is required in order to extrapolate model-scale laboratory testing to expected behavior in the field. At higher stress levels the dilatancy of soil is suppressed; relationships proposed by Bolton [9] are used to relate the critical state angle of friction to the peak angle of friction based on relative density and the stress state of the sand in the laboratory testing. Equations (2) and (3) are based on plane strain conditions for the relationship between critical and peak angles of friction based on the isotropic stress and density of the sample:

$$\phi'_{max} = 5I_R + \phi'_{cs} \tag{2}$$

$$I_R = I_D(10 - \ln p') - 1 \tag{3}$$

where ϕ'_{max} and ϕ'_{cs} are the peak and critical state friction angles, respectively, p' is the mean effective stress in the soil at failure and I_D is the relative density of the soil.

In order to validate the test results and sample preparation, a 90° piece (flat piece) was used to compare present measurements to published literature. The relative density of each test sample was calculated using the data presented in Table 1 which, in turn, was used to determine the value of ϕ'_{max}. Bearing failure was assumed to occur at 0.1B, neglecting soil cohesion and influence of overburden, the bearing capacity, q_{rd}, can therefore be defined as follows:

$$q_{rd} = {}^{1}/_{2}\, B N_\gamma \gamma' \tag{4}$$

where B is the width of the flat footing, N_γ is a bearing capacity factor and γ' is the effective unit weight of the soil.

Test results for the flat pieces are shown in Figure 7. Theoretical bearing loads are based on the approaches for calculating N_γ by Hansen [10] and Meyerhof [11]. Test results are consistent with theory and provide additional confidence in the experimental set up and the Bolton method [9].

Figure 8 shows an example of the incremental displacements in the soil obtained using PIV; the predicted failure plane according to Rankine theory, with a friction angle of 32°, has also been superimposed on the image. The sample in Figure 8 is for a dense sample which has a peak angle of friction of 45° when applying Equations (2) and (3). This is not consistent with the 32° overlaid as the dilation of the sand is suppressed at higher densities.

The development of a triangular active wedge beneath the footing, in addition to the passive wedges, is obvious from this output.

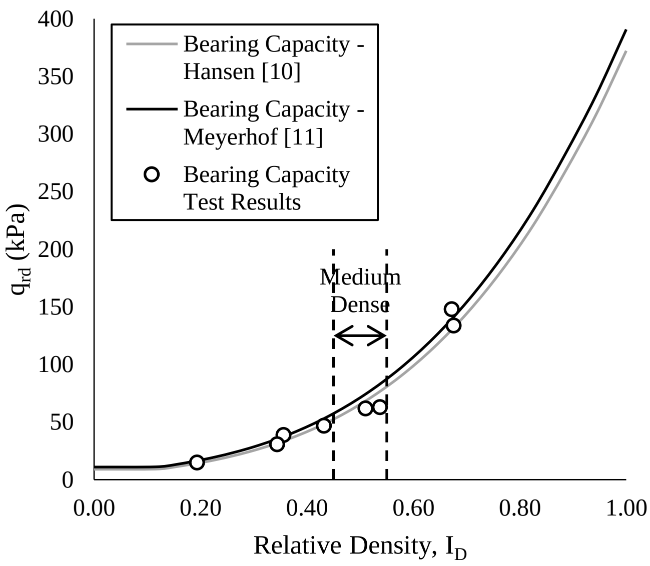

Figure 7 Theoretical and measured bearing capacities

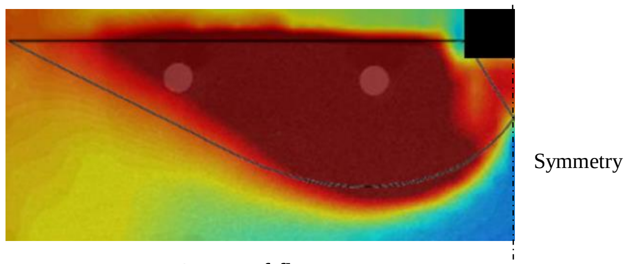

Figure 8 PIV of flat piece test

4 TESTING OF TAPERED ANGLE PIECES

A series of tests were carried out using cutting angles, β, of 30°, 45°, 60° and 75°. The test set-up for the cutting edges is shown in Figure 3. Each test was carried out on a medium-dense sample. The medium-dense tests have a relative density ranging between 0.44 and 0.54.

4.1 Influence of cutting angle, β

Figure 9 plots the influence of β on the variation of R with penetration. The resultant forces are higher for the shallower angles; this is attributable to the much greater bearing width of the flatter angles for the same penetration.

The influence of β on the relationship between Q_H and Q_V is examined in Figure 10 and Figure 11. The relationships presented in Figure 10 are remarkably linear where the steeper cutting angles reduce the vertical reaction. The ratio of horizontal to vertical force is shown in Figure 11 based on a best fit line to the results in Figure 10. In general, there appears to be a linear variation in Q_H/Q_V with β. It is worth noting that Q_H is as high as $0.9Q_V$ for a 30° cutting angle which could result in a large hoop tension force in the wall of the caisson.

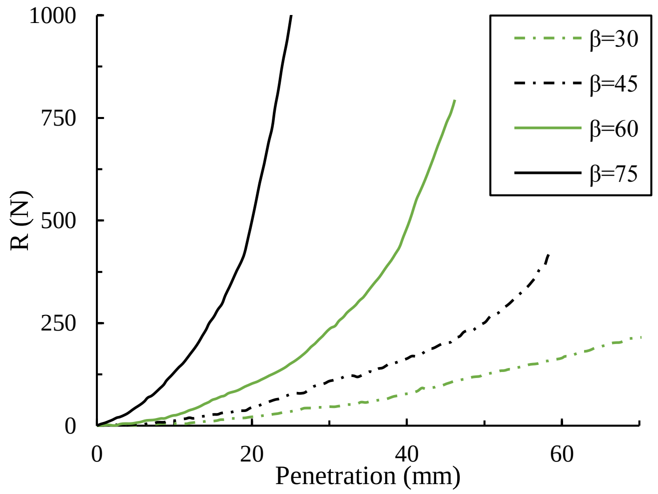

Figure 9 Resultant force of angle pieces

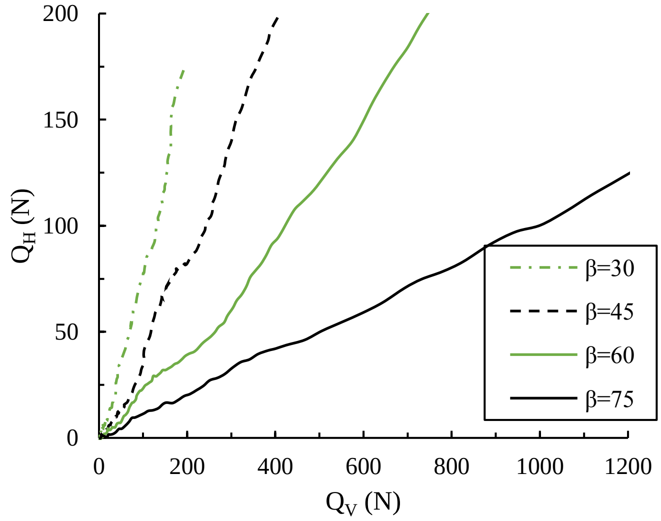

Figure 10 Horizontal against vertical forces

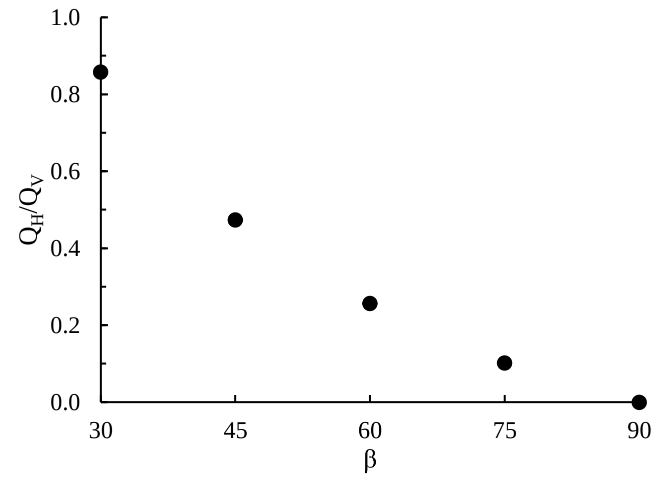

Figure 11 Ratio of Horizontal to vertical forces

Figure 12 shows the vertical bearing capacity of the footing, $q_{rd,v}$, against the embedment width. All angled footings illustrate a similar increase in bearing capacity with embedded width. The theoretical vertical bearing capacity of a flat footing is also plotted for various values of B. The bearing capacity of the flat footing is approximately 1.4 times the bearing capacity of the angle piece at values of B less than 50 mm. As the bearing pressure increases, there is a change in the rate in the increase of the bearing capacity. This could be attributable to the stress-state of the soil as penetration progresses; additional numerical work is being conducted to explore this aspect.

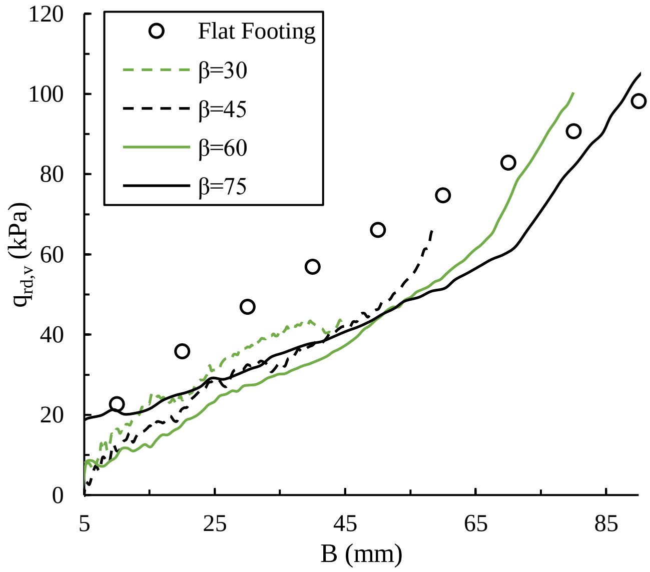

Figure 12 Effect of cutting angle on Nγ

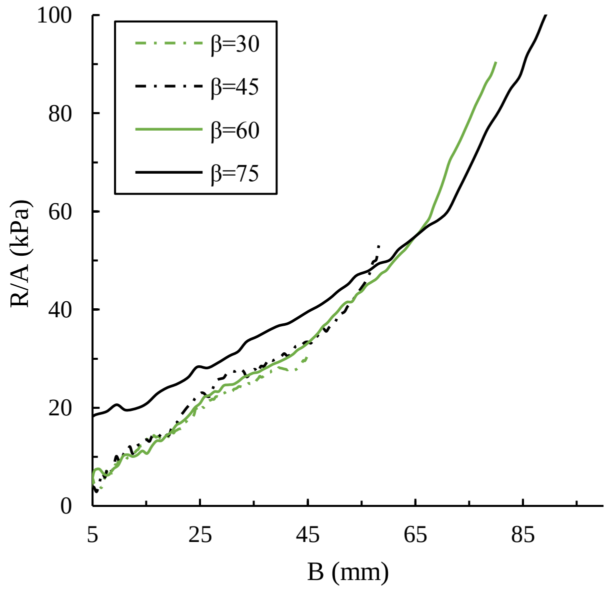

Figure 13 Average Face Pressure against footing width

In Figure 13, the variation of the pressure at the cutting face, R/A, is plotted against B. This framework appears to provide improved agreement between tests and appears to be relatively invariant to β. The slight differences in resultant pressures could be based on the slight differences in the relative densities and test discrepancies.

The failure mode for the different footing varies depending on the tapered angle, β. Figure 14 (a-d) shows the incremental total displacements of the soil; an embedment width of B=40 mm was chosen for these comparisons. At this stage of testing, the face pressures are similar (see Figure 13). The failure mechanism occurs towards the excavation side, as shown in Figure 14, as the tapered angles move into the active wedge of soil according to the Rankine theory for soil bearing failure. For the flatter angles, as the failure stresses in the soil develop, the soil begins to fail towards the excavation and overburden side, similar to a traditional flat footing.

Figure 15 show how the zone of influence varies with β. The depth and width of the failure zone is much higher for the steeper tapered angles at B=40 mm.

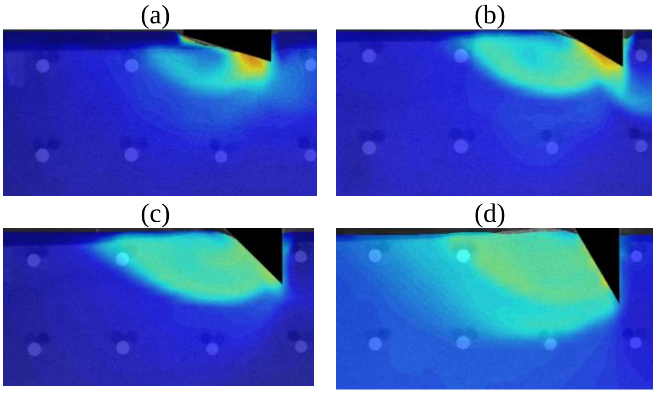

Figure 14 Resultant displacement at B=40mm: (a) β=75º, (b) β=60º, (c) β=45º, (d) β=30º

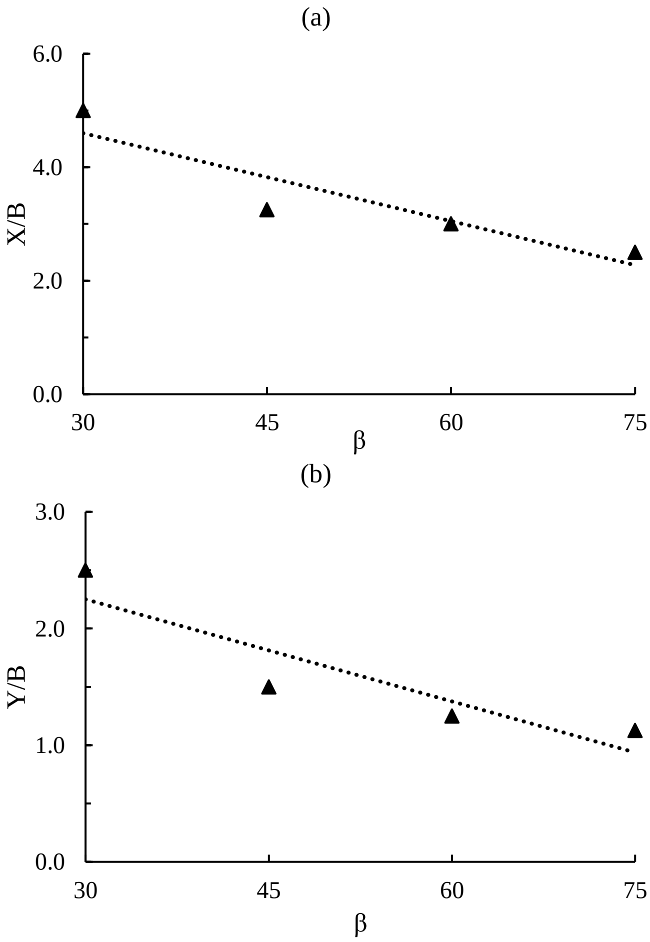

Figure 15 (a) Horizontal and (b) vertical zone of influence; B=40mm

4.2 Influence of overburden on one side

In the field, there will always be a surcharge outside the caisson from the overburden soil as excavation and sinking of the shaft commences. This surcharge will increase as the caisson sinks further into the ground. A surcharge was applied by applying a weight on the overburden side (see Figure 3). Surcharges of 12.5kPa, 25kPa and 50kPa were considered.

The overburden has two effects on the soil and the resulting failure mechanism. Firstly it increases the initial stress in the soil and secondly, it will encourage failure of the soil towards the excavation side. Figure 16 and Figure 18 shows the effects of the overburden against the base case of a level surface. It can be clearly seen that the overburden increases the bearing capacity of the soil beneath the footing.

The increase in bearing capacity is more sensitive to the shallower tapered angles, as the increase in resultant reaction is larger for β equal 75° compared to the β equal 45° test. The failure mechanism of the soil is shown in Figure 17 and Figure 19. For the higher surcharge pressures, the failure mechanism varies and is pushed towards the excavation side and the failure plane becomes larger.

The failure mechanism occurs towards the excavation side, as shown in Figure 14 for flatter angles (c-d), as the tapered angles move into the active wedge of soil according to the Rankine theory for soil failure. For the shallower tapered angles, as the failure stresses in the soil develop, the soil begins to fail towards the excavation and overburden side, similar to a traditional flat footing. This can be clearly seen in Figure 19 (g), as the soil failure mechanism develops on both sides of the 75° piece.

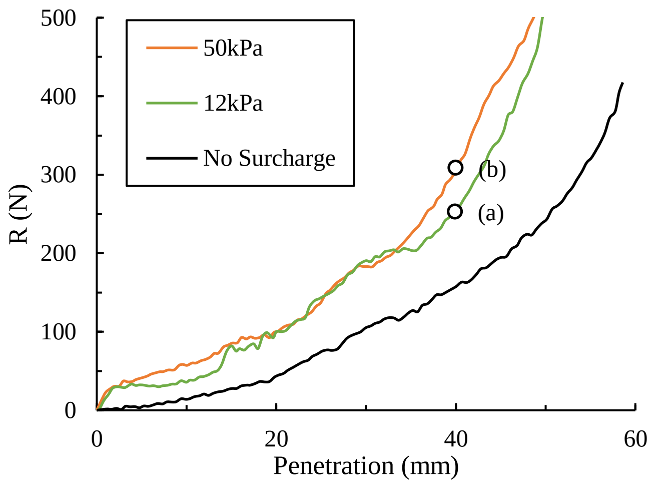

Figure 16 Influence of surcharge on resultant force; β=45,

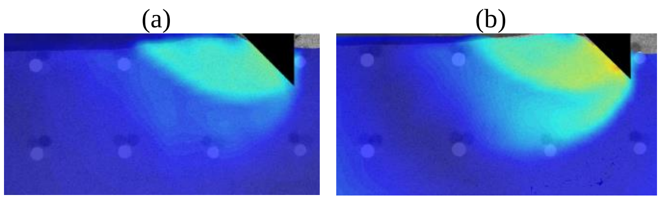

Figure 17 (a) 12kPa surcharge (b) 50kPa surcharge; B=40mm, β=45, see Figure 16

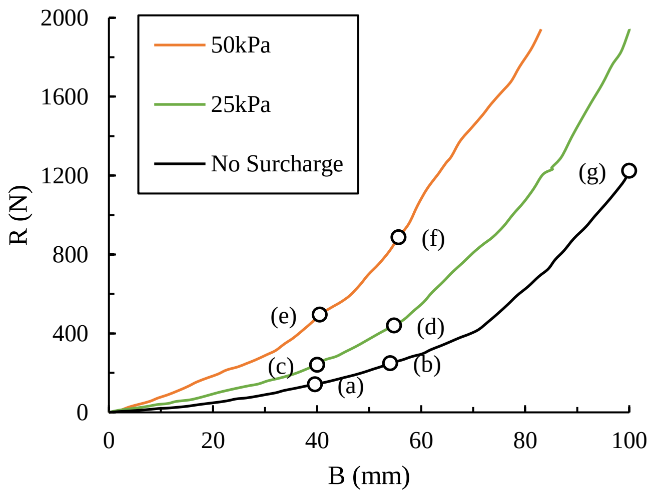

Figure 18 Influence of surcharge on resultant force; β=75,

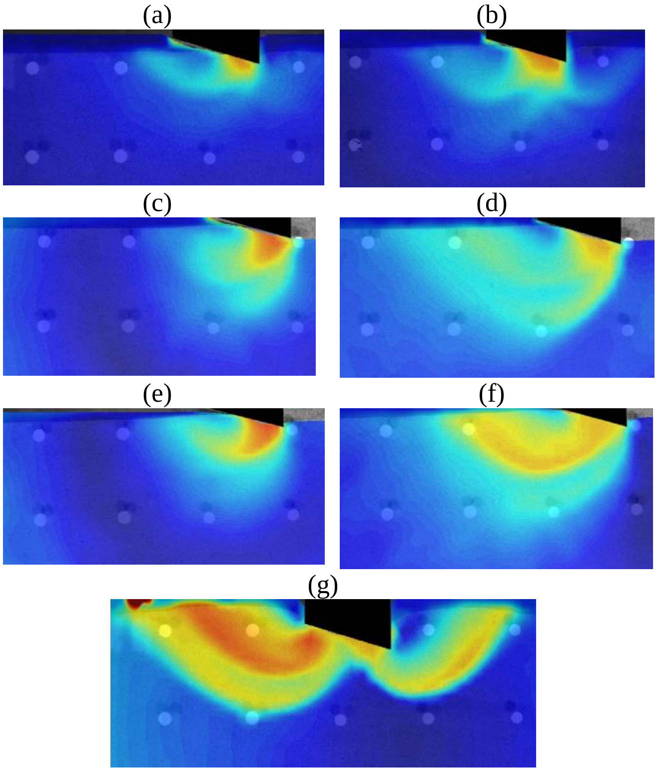

Figure 19 (a+b) No surcharge (c+d) 25kPa surcharge (e+f) 50kPa surcharge (g) No surcharge, B=100mm and 35mm penetration; β=75, see Figure 18

5 CONCLUSIONS

In this paper, a suite of tests carried out on small-scale tapered footings in medium-dense sand has been presented. The authors have arrived at the following conclusions arising from this study:

a) The forces that develop at the base of a caisson are largely dependent on the tapered angle of the footing. While steeper footings have a much reduced vertical resistance, at the same penetration, this is offset by an increase in the horizontal reaction. The bearing pressure on the face of the footing appears to be invariant to the cutting angle of the test piece and varies linearly with the embedment width of the piece.

b) Applying an overburden pressure on one side of the footing best models conditions in the field. The overburden has a greater influence on flatter cutting angles since failure wedges are developed on both sides of the cutter unlike steep angles where the failure wedge develops on the excavation side only. The overburden forces failure to occur on the excavation side, thereby increasing the bearing capacity.

c) Output from the PIV analysis of the present tests can be used to guide excavation on site in order to induce failure of the soil beneath the caisson.

d) Further work is being carried out at University of Oxford to extend these results and confirm the applicability to conditions in the field. In particular, further comparisons with full-scale measurements will be carried out to ensure that the proposed methods are reliable and valid.

ACKNOWLEDGMENTS

The authors gratefully acknowledge the financial support provided by Ward and Burke Construction Ltd.

REFERENCES

[1] M. J. Cassidy and G. T. Houlsby, “Vertical bearing capacity factors for conical footings on sand,” *Géotechnique*, no. 52, pp. 687–692, 2002.

[2] G. T. Houlsby and C. M. Martin, “Undrained bearing capacity factors for conical footings on clay,” *Geotechnique*, vol. 53, no. 5, pp. 513–520, 2003.

[3] M. J. Tomlinson, *Foundation Design and Construction*, 7 edition. Harlow, England; New York: Prentice Hall, 2001.

[4] E. Nonveiller, “Open caissons for deep foundations,” *J. Geotech. Eng.*, vol. 113, no. 5, pp. 424–439, 1987.

[5] N. B. Solov’ev, “Use of limiting-equilibrium theory to determine the bearing capacity of soil beneath the blades of caissons,” *Soil Mech. Found. Eng.*, vol. 45, no. 2, pp. 39–45, 2008.

[6] F. Y. Yan, Y. C. Guo, and S. Q. Liu, “The Bearing Capacity Analyses of Soil beneath the Blade of Circular Cassion,” in *Advanced Materials Research*, 2011, vol. 250, pp. 1794–1797.

[7] C. M. Martin, “Physical and numerical modelling of offshore foundations under combined loads,” University of Oxford, 1994.

[8] S. A. Stanier, J. Blaber, W. A. Take, and D. White, “Improved image-based deformation measurement for geotechnical applications,” *Can. Geotech. J.*, no. ja, 2015.

[9] M. D. Bolton, “The strength and dilatancy of sands,” *Geotechnique*, vol. 36, no. 1, pp. 65–78, 1986.

[10] J. Hansen, “A general formula for bearing capacity, Danish Geotechnical Institute Bulletin,” *No.(11)*, 1961.

[11] G. G. Meyerhof, “Some recent research on the bearing capacity of foundations,” *Can. Geotech. J.*, vol. 1, no. 1, pp. 16–26, 1963.